J Mol Model (2010) 16:1307–1318
DOI 10.1007/s00894-010-0646-3

ORIGINAL PAPER

Distinct interactions between the human adrenergic β_2 receptor and Gα_s—an in silico study

Andrea Straßer · Hans-Joachim Wittmann

Received: 13 August 2009 / Accepted: 21 December 2009 / Published online: 30 January 2010

Abstract The aim of this study was to perform an in silico analysis of the interaction of the human β_2 adrenergic receptor with Gα_s. In a first step, a systematic surface-interaction-scan between the inactive or active human β_2 adrenergic receptor and Gα_s was performed in order to gain knowledge about energetically preferred areas on the potential energy surface. Subsequently, two energetically favored regions for the active human β_2 adrenergic receptor–Gα_s complex were identified. Two representative complex structures were put into a POPC (1-palmitoyl-2-oleoyl-phosphatidylcholine) bilayer and solvated in order to perform molecular dynamic simulations. The simulations revealed that both conformations, which have comparable potential energy, are stable. A mean number of about 14 hydrogen bonds was observed between the active receptor and Gα_s for both conformations. Based on these results, two energetically favored β_2–G$\alpha_s$complexes can be proposed.

Keywords Adrenergic β_2 receptor · Gα_s subunit · Receptor-G-protein interaction · Energy surface scan · Molecular dynamics

Introduction

G-protein-coupled receptors (GPCRs) are important targets for several drugs [1]. They consist of seven transmembrane (TM) domains, connected by intra- and extracellular loops, and couple intracellular proteins to G proteins, which consist of Gα, Gβ and Gγ subunits [2, 3]. These heterotrimeric G proteins act as switches on a molecular level, turning on intracellular signal cascades, induced by activation of the corresponding GPCR [4, 5]. The α subunit (Gα_s) is able to switch between its inactive GDP (guanosindiphosphate)-bound conformation and its active GTP (guanosintriphosphate)-bound conformation. Recent crystallographic studies have given insight into the structure of both GPCRs and G proteins [6–11]. But still no crystal structure of a complete GPCR–G protein complex is available. However, some experimental studies have provided hints as to the interactions between GPCR and the Gα_s of the G protein [12].

Two opposite models regarding GPCR–G protein coupling have been proposed. One model—the "collision coupling" model—suggests that G-proteins interact only with receptors in the active state [13]. In contrast, the second model suggests that G proteins are able to interact with the GPCR before the GPCR has been activated by an agonist. This means that the GPCR and G protein are pre-coupled. Several studies have provided evidence supporting the pre-coupled model [14–16]. Experimental studies identified regions of GPCR and G-protein that interact with each other. It is thought that, during activation of GPCR, a pocket in the intracellular part of the receptor is opened, which interacts with the C-terminus of Gα_s [12, 17]. Further mutagenesis studies identified amino acids of the α4–β6 [18–23] and α3–β5 [24] loops as being involved in interaction with the GPCR. Additionally, it was shown that the N-terminus of Gα_s interacts with GPCRs [20, 25–28]. Thus, experimental studies have provided information about receptor-G-protein interaction sites. However, all experimentally

A. Straßer (✉) · H.-J. Wittmann
Department of Pharmaceutical and Medicinal Chemistry,
Faculty of Chemistry and Pharmacy, University of Regensburg,
Universitätsstraße 31,
93040 Regensburg, Germany
e-mail: andrea.strasser@chemie.uni-regensburg.de

detected receptor-G-protein interactions cannot be explained by a single model [29]. Thus, it is suggested that receptor dimers may play a role, or that sequential interactions between receptor and G-protein take place [30, 31].

Until now, only a few in silico studies have been performed to gain insight into possible interactions between G-proteins and their receptors [32–37]. The aim of this study was to perform an in silico simulation of the interaction between the human adrenergic β_2 receptor ($h\beta_2R$) with the $G\alpha_s$-subunit. First, a systematic scan of the potential energy surface between inactive or active $h\beta_2R$ and $G\alpha_s$ was performed. Subsequent analysis of the surface scan showed that a large number of conformations of pre-coupled inactive $h\beta_2R$–$G\alpha_s$ complexes are localized on the same energetic level. In contrast, for the active $h\beta_2R$–$G\alpha_s$ complex, two conformations are energetically favored. To gain detailed information about distinct interactions between $h\beta_2R$ and $G\alpha_s$, an inactive $h\beta_2R$–$G\alpha_s$ complex and the two favored active $h\beta_2R$–$G\alpha_s$ complexes were embedded in their natural surroundings, including lipid bilayer and water. Subsequently, molecular dynamic simulations were performed.

Methods

Modeling of the inactive and active conformation of $h\beta_2R$

For modeling the inactive conformation of the $h\beta_2R$ (Fig. 1), we used the corresponding crystal structure (2RH1.pdb) [7–9]. Based on the crystal structure of the active state of opsin, coupled to 11 amino acids of the C-terminus of Gα (3DQB.pdb) [12], a model of the active state $h\beta_2R$ was generated by homology modeling. This homology modeling was performed using the software SYBYL 7.0 (Tripos; http://www.tripos.com/). The alignment between $h\beta_2R$ and opsin is based on the highly conserved amino acids of each TM domain as described [38]. Loops exhibiting different lengths between $h\beta_2R$ and opsin were modeled using the loop search module of SYBYL 7.0. Since the E2 loop of the $h\beta_2R$ is significantly different from the E2 loop conformation of opsin, as confirmed by the corresponding crystal structures of the inactive $h\beta_2R$ and opsin, the E2 loop from 2RH1.pdb was adopted. Since the crystal structure supplies no information about the conformation of the I3 loop or C-terminus, both were not fully included into the model. We did not model amino acids

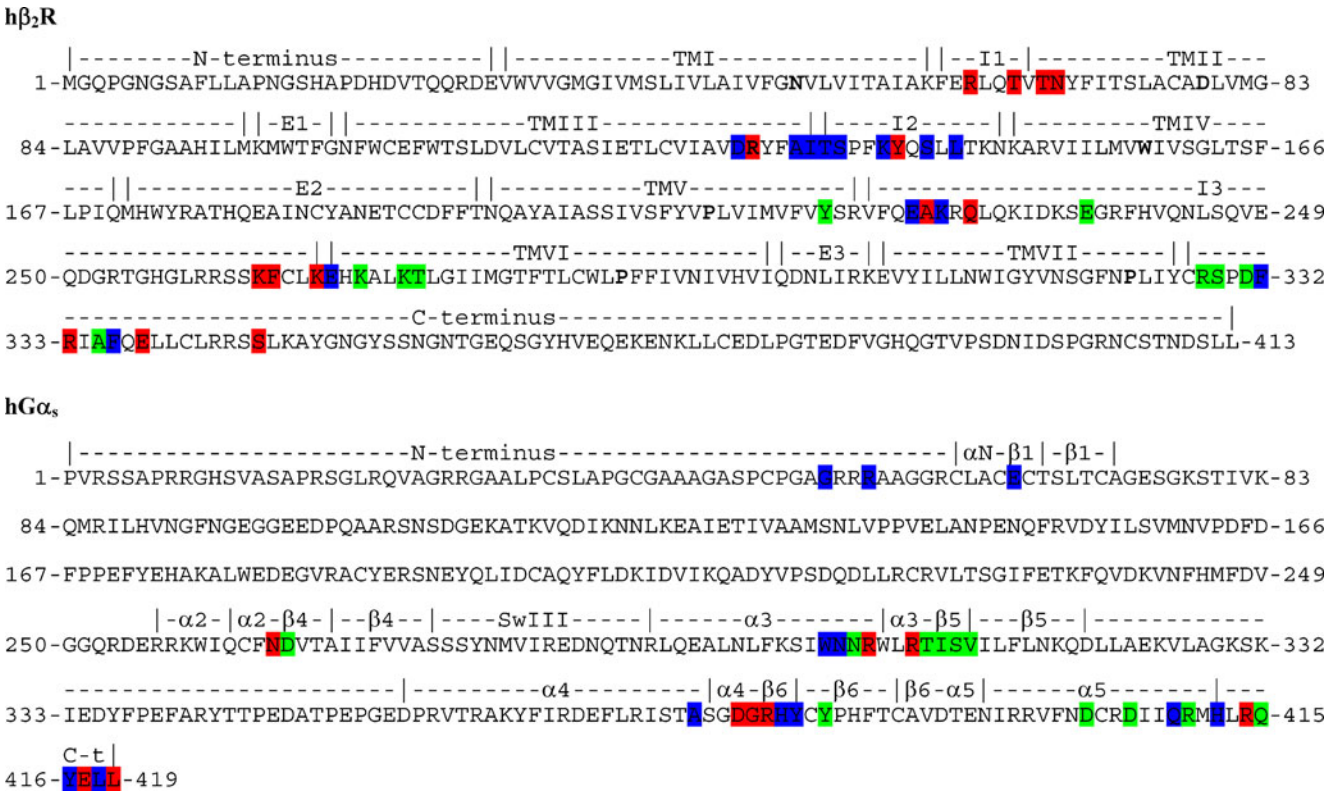

Fig. 1 Amino acid sequences of the human β_2 adrenergic receptor ($h\beta_2R$) and human G protein α subunit ($G\alpha_s$). In $h\beta_2R$, highly conserved amino acids (according to [38]) are given in *bold*. All amino acids establishing an interaction during the productive phase of the molecular dynamics (MD) simulation between $h\beta_2R$ and $G\alpha_s$ are given in colored boxes: *green* model I, *blue* model II, *red* models I and II

232–262 of the I3-loop (Fig. 1); instead, we closed the I3-loop by connecting amino acids 231 and 263 with six alanines. The C-terminus was modeled up to amino acid 346 (Fig. 1).

Construction of $G\alpha_s$ in the GDP-bound state

Since no crystal structure of the GDP-bound state of $G\alpha_s$ is available, a model of the GDP-bound state of $G\alpha_s$ was constructed by comparative homology modeling, using the heterotrimeric GDP-bound state of $G\alpha_{i1}$ (1GP2.pdb) [39] as template. Modeling was performed as described previously [32].

Construction of $G\alpha_s$ in the GTP-bound state

The crystal structure of $G\alpha_s$ (1AZT.pdb) [40] with GTPγS bound was used to model $G\alpha_s$ (Fig. 1) in the GTP-bound state. Since there is no complete N-terminus in 1AZT.pdb, 1AZT.pdb was aligned to 1GG2.pdb [41] and the N-terminus of 1GG2.pdb was transferred to 1AZT.pdb. Additionally, the missing amino acids in the C-terminus were added in a helical conformation. Furthermore, the missing amino acids 91–112 were adopted from 1GG2.pdb. Amino acids were mutated into the corresponding amino acid of $hG\alpha_s$ where appropriate.

Construction and surface scan of the inactive and active $h\beta_2R$-$G\alpha_s$-complexes

An in-house surface-scan routine was used to dock $G\alpha_s$ to $h\beta_2R$. Therefore, a starting structure was needed. This was generated by manual positioning of $G\alpha_s$ below the intracellular part of inactive or active $h\beta_2R$. In the next step, a surface-scan of the contact surface between the intracellular part of $h\beta_2R$ and $G\alpha_s$ was performed using the in-house surface-scan routine: the position of $h\beta_2R$ was fixed and only $G\alpha_s$ was translated in the *x*-, *y*- and *z*-directions and rotated about the *x*-, *y*- and *z* axes systematically, always using the described starting structure as a starting point (Fig. 2). The surface scan was performed for inactive and active $h\beta_2R$–$G\alpha_s$-complexes. Nine points with an increment of 0.25 nm were used to scan in the *x*- and *y*-direction, respectively. In the *z*-direction, 17 points with an increment of 0.125 nm were established. For rotation about the *z*-axis, 12 points with an angle increment of 30 degrees were used; for rotation about the *x*- and *y*-axis, 5 points with an increment of 15 degrees were used. Thus, within this scan, about 400,000 structures were generated. After analyzing these results with regard to potential energy of the active $h\beta_2R$-$G\alpha_s$–complex, two distinct regions hinting at local minima were identified. In order to localize the two minima more exactly, a refined scan was performed in these two regions, using 9 points with an increment of 0.05 nm in the *x*-, *y*- and *z*-direction, respectively. Rotation about the *z*-axis was refined by 7 points with an increment of 10 degrees. Rotation about the *x*- and *y*-axis was refined by 5 points with an increment of 7.5 degrees. Thus, for both refined scans, about 125,000 structures were calculated. To sum up, more than 650,000 structures for the active $h\beta_2R$–$G\alpha_s$ complex were calculated. The surface scan did not reveal significant minima for the inactive $h\beta_2R$–$G\alpha_s$ complex, thus a refined scan was not performed. After each structure generation, the resulting $h\beta_2R$–$G\alpha_s$ complex was completely energy minimized with Gromacs [42], using the ffG53A6 force field [43] for the protein. Energy minimization, using the steepest decent method, was performed for a maximum of 10,000 steps, or until a maximum force smaller than 100 kJ mol^{-1} nm^{-1} was achieved. The distances for coulomb cutoff and Lennard-Jones cutoff were set to 1.4 nm. Thereby, all sites were

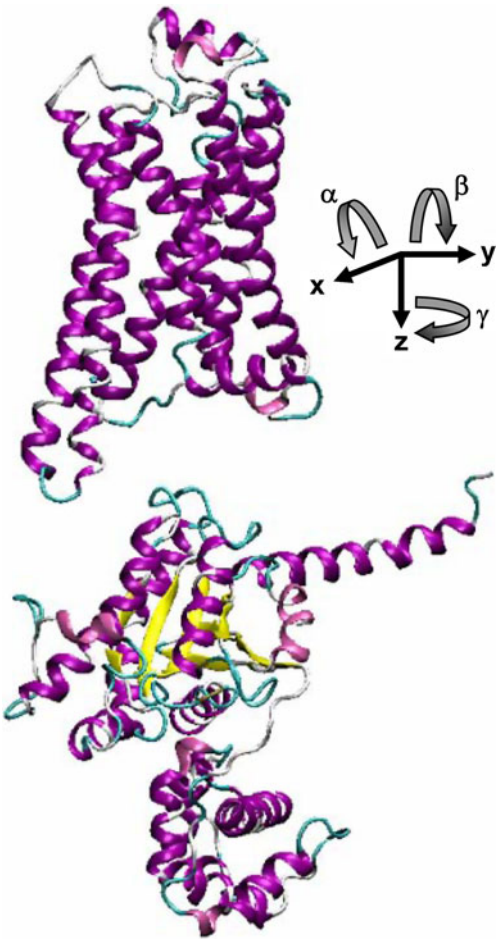

Fig. 2 Axis system for the $h\beta_2R$–$G\alpha_s$ complex

allowed to be minimized, i.e., no position constraints were set.

Molecular dynamics simulations of the hβ$_2$R–Gα$_s$ complex in natural surroundings

To gain detailed insight into the interactions between inactive hβ$_2$R and the GDP-bound state of Gα$_s$, the complex with lowest potential energy was embedded in a POPC (1-palmitoyl-2-oleoyl-phosphatidylcholine) bilayer (10 nm×10 nm) containing 218 POPC molecules. Subsequently, the whole simulation box (10 nm×10 nm×12 nm) was filled with 30,555 spc (single point charge) water [44] molecules. The resulting system, containing about 110,000 sites, was energetically minimized (maximum 10,000 steps, or until a maximum force smaller than 100 kJ mol^{-1} nm^{-1} was achieved; the distances for coulomb cutoff and Lennard-Jones cutoff were set to 1.4 nm; all sites were allowed to be minimized; no position constraints were set) and then used as a starting structure for the molecular dynamics (MD) simulation. The same steps were performed for the two energetically favored active hβ$_2$R–Gα$_s$ complexes with completely different conformations. All MD simulations were performed with Gromacs [42]. For all simulations, rectangular periodic boundary conditions were used. The particle mesh Ewald (PME) method [45] was applied to describe the electrostatic interactions. The distances for coulomb

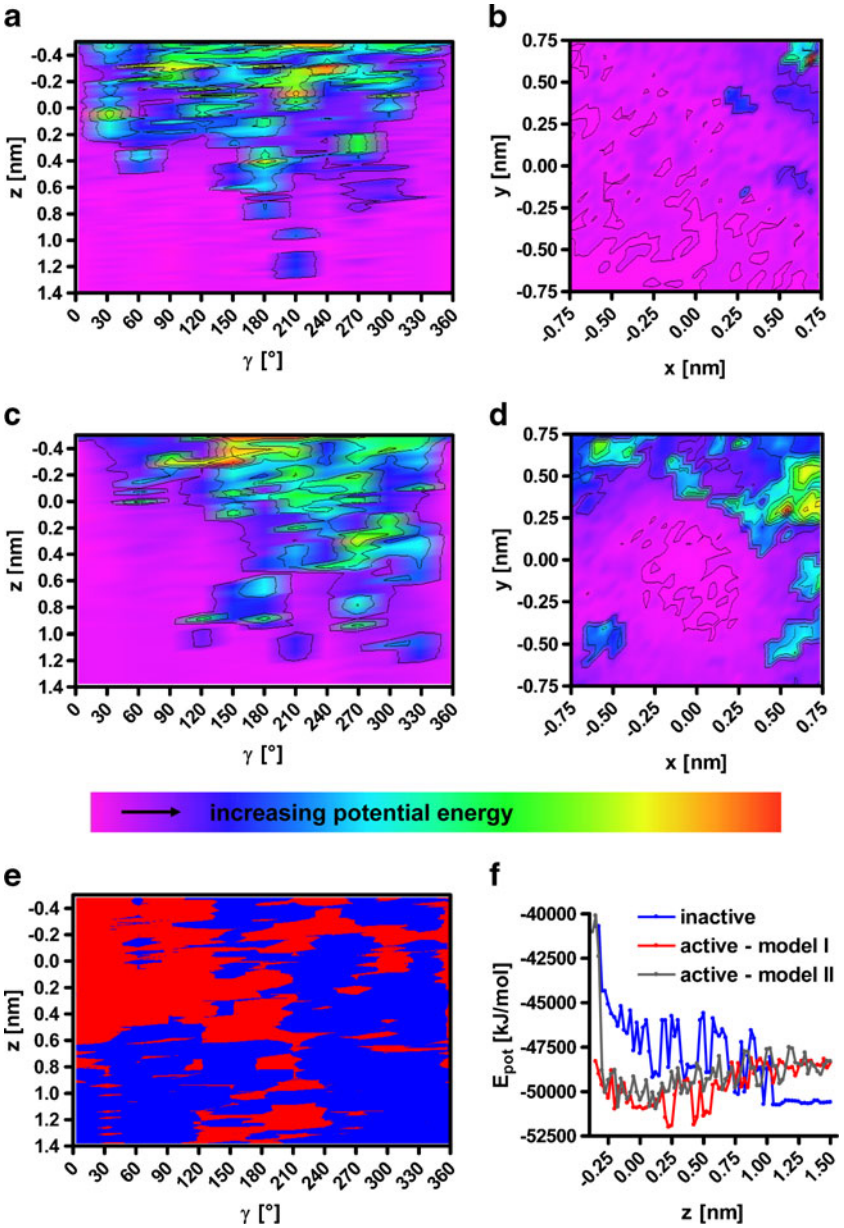

Fig. 3 Calculated potential energy surfaces between hβ$_2$R and G$_s$α. **a** Inactive hβ$_2$R and Gα$_s$; *z* variation of the distance between hβ$_2$R and Gα$_s$; γ rotation of Gα$_s$ around the z axis. **b** Inactive hβ$_2$R and translation of Ga$_s$ in the xy-plane at distinct z, α, β and γ. **c** Active hβ$_2$R and Gα$_s$; *z* variation of the distance between hβ$_2$R and Gα$_s$; γ rotation of Gα$_s$ around the *z* axis. **d** Active hβ$_2$R and translation of Gα$_s$ in the xy-plane at distinct z, α, β and γ. **e** *z* variation of the distance between hβ$_2$R and Gα$_s$; γ rotation of Gα$_s$ around the z axis; distinct x, y, α and β; *red areas* with the active-hβ$_2$R–Gα$_s$ complex being energetically preferred; *blue areas* with the inactive-hβ$_2$R–Gα$_s$ complex being energetically preferred. **f** Potential energy for the inactive-hβ$_2$R–Gα$_s$ (*blue*) and active-hβ$_2$R–Gα$_s$ (*red*) complex, according to model I and active hβ$_2$R–Gα$_s$ (*grey*) complex, according to model II, in dependence of variation of distance z between receptor and Gα-subunit

cutoff and Lennard-Jones cutoff were set to 1.4 nm. The dielectric constant was set to 1. For all simulations, a timestep of 2 fs was used. The list of non-bonded atoms pair list was updated every 10 fs. The simulation temperature was 310 K and the pressure 1 bar. In the equilibration phase, berendsen temperature (time constant 0.1 ps) and pressure (time constant 0.5 ps) coupling were used [46]. In the subsequent productive phase, the Nose-Hoover thermostat [47, 48] was used for temperature (time constant 1 ps) and the Parinello-Rahman barostat (time constant 1 ps) [49] for pressure coupling. A 2,550-ps equilibration phase with position constraints onto backbone (bb) and sidechain (sc) atoms of the $h\beta_2R$ and $G\alpha_s$ was performed. Therefore, the simulation was divided into 12 cycles with the following position constraints in kJ/(mol nm^2): cycle 1: 500 ps, bb 5,000, sc 5,000; cycle 2: 250 ps, bb 5,000, sc 4,000; cycle 3: 250 ps, bb 4,000, sc 3,000; cycle 4: 250 ps, bb 3,000, sc 2,000; cycle 5: 150 ps, bb 2,000, sc 1,000; cycle 6: 150 ps, bb 1,000, sc 800; cycle 7: 150 ps, bb 800, sc 600; cycle 8: 150 ps, bb 600, sc 400; cycle 9: 150 ps, bb 400, sc 200; cycle 10: 150 ps, bb 200, sc 100; cycle 11: 150 ps, bb 100, sc 0; cycle 12: 250 ps, bb 0, sc 0. After the 2,550 ps equilibration phase, a 2,500 ps productive phase without any position constraints was performed.

Results and discussion

Surface scan of the inactive and active $h\beta_2R$–$G\alpha_s$ complex

The results of the potential energy surface scan are presented in Fig. 3. The section of the energy surface with variation of the distance, z, between the inactive $h\beta_2R$ and $G\alpha_s$, and also the rotation of $G\alpha_s$ around the z axis (Fig. 3a) shows a wide plain with rather small potential energy for a distance $z>0.6$ nm of the $G\alpha_s$ C-terminus with respect to the reference position. An increasing distance z leads to a decrease in potential energy. In contrast, for a decrease in z, a significant increase in potential energy was observed. This increase in potential energy can be explained by the fact that there is not enough space between the intracellular parts of the TM domains of the inactive $h\beta_2R$. Consequently, the C-terminus of $G\alpha_s$ cannot penetrate between the helices of the receptor. For $z=0.075$ nm, the potential energy as function of translation of the $G\alpha_s$ in x- and y-direction is given (Fig. 3b). Here, the potential energy is a wide plain, with a significant increase at only some positions. This result can be explained by the fact that the $G\alpha_s$ shows only a slight contact to the inactive $h\beta_2R$, without penetration of the C-terminus between the TM domains at the given z. Thus, $G\alpha_s$ can move on the intracellular receptor surface without steric collision. The potential energy surface of the active $h\beta_2R$ and $G\alpha_s$, with a variation of the distance z between receptor and $G\alpha_s$ and a rotation of $G\alpha_s$ around the z axis was significantly different to that of the inactive $h\beta_2R$ (Fig. 3c). Minima in potential energy were found for $z<0.5$ nm, especially for values of z between 0.0 nm and 0.25 nm. For distances z in this range, only a slight rotation of the $G\alpha_s$ around the z axis, without a large increase in potential energy, was possible. This minimum is defined as model I (Fig. 4). In this model, the N-terminus of $G\alpha_s$ is located below TM II of the receptor. The $G\alpha_s$ subunit is located in the large space between TM VI and TM VII of the receptor (Fig. 4). An increase in the distance $z>0.6$ nm led to a slight increase in potential energy, due to the fact that for a larger distance the interaction energy between the active $h\beta_2R$ and the $G\alpha_s$ was lost. For z from about 0.6 nm to 1.0 nm, a second local, but energetically higher minimum area was identified for γ ranged between 210°–240°. In this small area, a further $h\beta_2R$–$G\alpha_s$ complex can be located, but due to the z being from 0.6 nm to 1.0 nm, there was no penetration of the

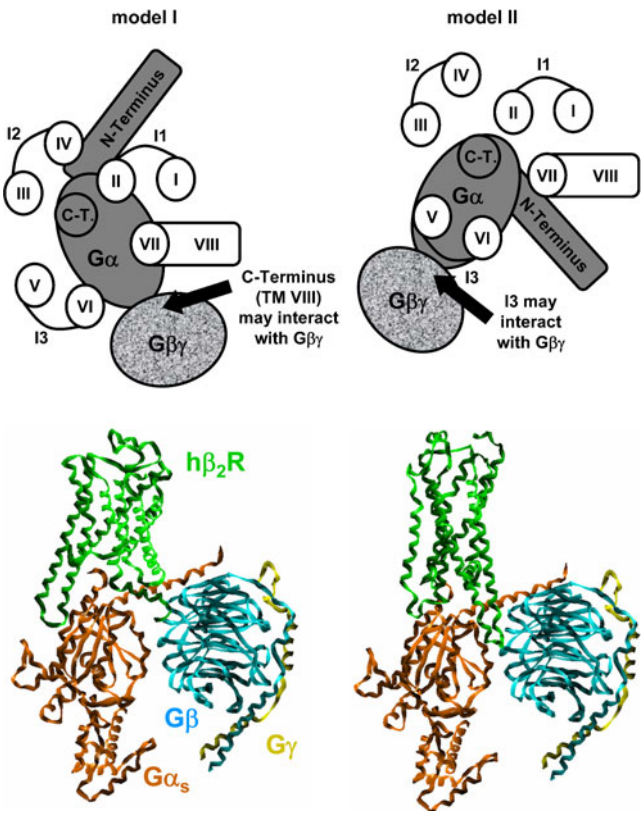

Fig. 4 Two schematic models for preferred receptor–G-protein interaction. Model I: the Gβγ-interaction site of the Gα is located between transmembrane (TM) domain VI and TM VII of the receptor. In this model, a long C-terminus may interact with the Gβγ subunit and thus stabilize the receptor–G-protein complex. Model II: the Gβγ-interaction site of the $G\alpha_s$ is located between TM V and TM VI. Thus, in this model, a long I2-loop may interact with the Gβγ subunit in order to stabilize the receptor-G-protein-complex

$G\alpha_s$-C-terminus between the TMs of the receptor, as indicated by the crystal structure. But further investigations at γ, ranged between 210°–240° but with different x, y, α and β, identified another local minimum, with a possible penetration depth of the C-terminus of $G\alpha_s$ of around $z \approx 0$ (corresponding section of the energy surface not shown). This minimum is defined as model II (Fig. 4). In model II, the N-terminus of $G\alpha_s$ is located between TM VI and TM VII of the receptor, and the $G\alpha_s$ subunit is located below TM V and TM VI of the receptor (Fig. 4). In general, the potential surface scan can find two energetically favored minima on the potential energy surface. These correspond to two different binding models for the active $h\beta_2R$–$G\alpha_s$ complex. For $z=0.25$ nm, the potential energy with translation of $G\alpha_s$ in the x- and y-direction is shown (Fig. 3d). In contrast to the inactive complex, the potential energy increased significantly with small translation steps in the x- or y-direction. This is in good agreement with the fact that part of the $G\alpha_s$ C-terminus is located in a small pocket between the TM domains of the receptor. Thus, small translations lead to collisions with the receptor. The regions—dependent on distance z and rotation about the z axis—that are more stable for the inactive $h\beta_2R$–$G\alpha_s$ (blue) and active $h\beta_2R$–$G\alpha_s$ complex

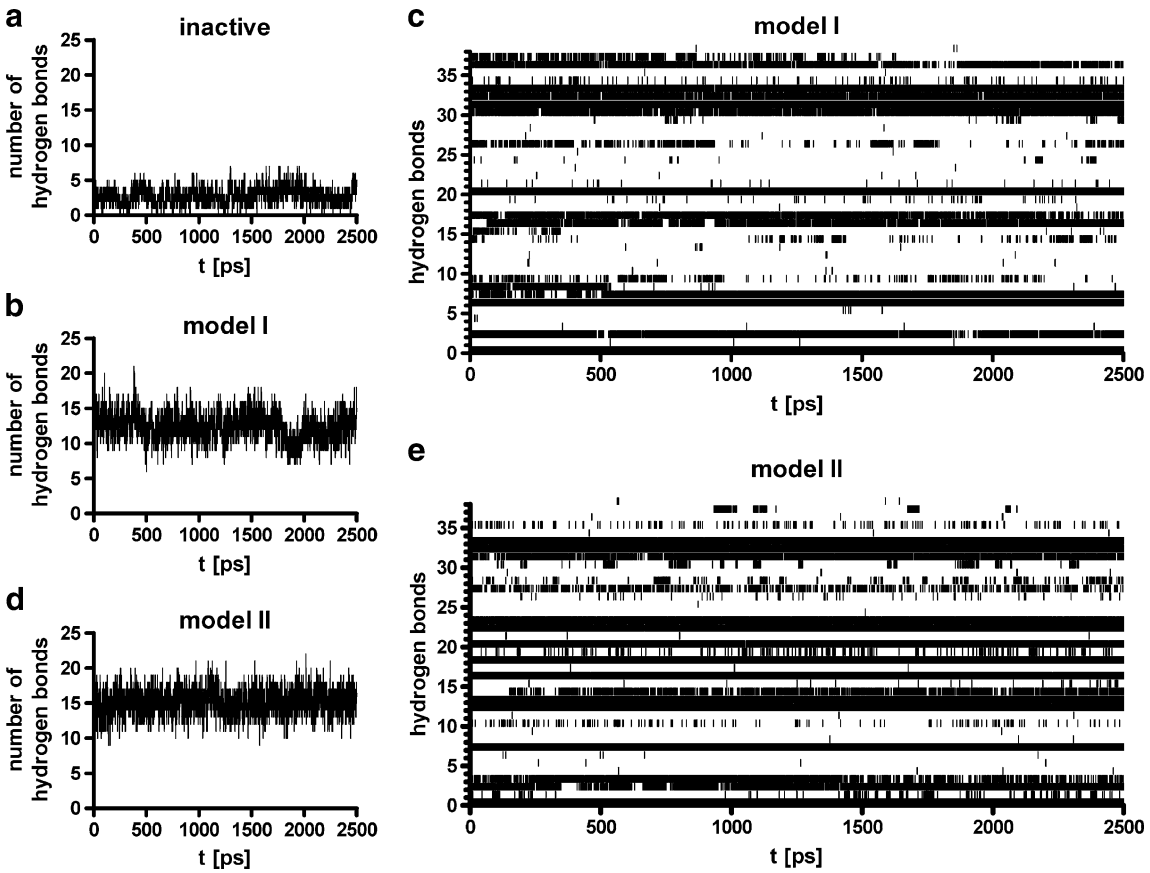

Fig. 5 Hydrogen bond interactions between $h\beta_2R$ and $G\alpha_s$. **a** Number of hydrogen bonds during the 2.5 ns productive phase of MD simulation of the inactive $h\beta_2R$–$G\alpha_s$ complex. **b** Number of hydrogen bonds during the 2.5 ns productive phase of MD simulations of the active $h\beta_2R$–$G\alpha_s$ complex, according to model I. **c** Distinct hydrogen bond interactions between the active $h\beta_2R$ and $G\alpha_s$ during the 2.5 ns productive phase of MD, according to model I: *1* 63R–264N, *2* 63R–265D, *3* 63R–415Q, *4* 66T–417E, *5* 68T–416Y, *6* 68T–417E, *7* 69N–417E, *8* 131R–417E, *9* 131R–419L, *10* 141Y–410R, *11* 219Y–419L, *12* 226A–414R, *13* 229Q–406D, *14* 229Q–410R, *15* 229Q–414R, *16* 237E–403D, *17* 263K–311S, *18* 263K–312V, *19* 263K–385Y, *20* 264F–385Y, *21* 267K–385Y, *22* 267K–414R, *23* 267K–415Q, *24* 270K–380G, *25* 270K–381R, *26* 273K–379D, *27* 274T–417E, *28* 328R–381R, *29* 329S–381R, *30* 331D-308R, *31* 331D–309T, *32* 331D–310I, *33* 285D–415Q, *34* 333R–417E, *35* 335A–308R, *36* 338E–305R, *37* 338E–308R, *38* 346S–304N. **d** Number of hydrogen bonds during the 2.5 ns productive phase of MD simulations of the active $h\beta_2R$–$G\alpha_s$ complex, according to model II. **e** Distinct hydrogen bond interactions between the active $h\beta_2R$ and $G\alpha_s$ during the 2.5 ns productive phase of MD, according to model II: *1* 63R–409Q, *2* 63R–412H, *3* 63R–66E, *4* 66T–414R, *5* 68T–414R, *6* 68T–418L, *7* 69N–417E, *8* 130D–381R, *9* 131R–381R, *10* 134A–381R, *11* 135I–381R, *12* 136T–379D, *13* 137S–379D, *14* 140K–376A, *15* 141Y–302W, *16* 141Y–379D, *17* 141Y–380G, *18* 141Y–382H, *19* 143S–383Y, *20* 145L–383Y, *21* 145L–414R, *22* 225E–308R, *23* 226A–305R, *24* 227K–305R, *25* 229Q–303N, *26* 229Q–305R, *27* 229Q–308R, *28* 263K–264N, *29* 264F–305R, *30* 267K–264N, *31* 268E–305R, *32* 332F–416Y, *33* 333R–417E, *34* 333R–419L, *35* 336F–416Y, *36* 338E–56R, *37* 346S–53G, *38* 346S–56R

(red), respectively, are given (Fig. 3e). The potential energy for y=0 nm with variation of z is given (Fig. 3f). The inactive $h\beta_2R$–$G\alpha_s$ complex has, compared to the active $h\beta_2R$–$G\alpha_s$ complexes (model I and II), lower potential energy for large values of z>0.85 nm. But for values of z<0.75 nm, the potential energy of the active $h\beta_2R$–$G\alpha_s$ complex is smaller compared to the inactive $h\beta_2R$–$G\alpha_s$ complex.

Hydrogen bond network between $h\beta_2R$ and $G\alpha_s$

To gain detailed insight into the hydrogen bond networking (Fig. 5) between the inactive $h\beta_2R$ and $G\alpha_s$ on the one hand, and the active $h\beta_2R$ and $G\alpha_s$ on the other, MD simulations were performed. For the inactive $h\beta_2R$–$G\alpha_s$ complex only a small number of hydrogen bonds, ranging between zero and seven, were observed. This corresponds

Table 1 Hydrogen bond interactions between human β_2 adrenergic receptor ($h\beta_2R$) and human G protein α subunit ($G\alpha_s$). *TM* Transmembrane

	Model I		Model II	
	Interaction sites $h\beta_2R$–$G\alpha_s$	[%]	Interaction sites $h\beta_2R$–$G\alpha_s$	[%]
1	63R (I1)–264N (α2-β4)	0.2	63R (I1)–409Q (α5)	10.3
2	63R (I1)–265D (α2-β4)	83.9	63R (I1)–412H (α5)	82.3
3	63R (I1)–415Q (C-term)	0.2	63R (I1)–66E (αN-β1)	51.5
4	66T (I1)–417E (C-term)	0.1	66T (I1)–414R (C-term)	0.2
5	68T (TMII)–416Y (C-term)	0.2	68T (TMII)–414R (C-term)	0.2
6	68T (TMII)–417E (C-term)	99.2	68T (TMII)–418L (C-term)	0.2
7	69N (TMII)–417E (C-term)	86.1	69N (TMII)–417E (C-term)	99.9
8	131R (TMIII)–417E (C-term)	16.9	130D (TMIII)–381R (α4-β6)	0.2
9	131R (TMIII)–419L (C-term)	14.4	131R (TMIII)–381R (α4-β6)	0.1
10	141Y (I2)–410R (α5)	0.2	134A (TMIII)–381R (α4-β6)	6.2
11	219Y (TMV)–419L (C-term)	0.4	135I (TMIII)–381R (α4-β6)	0.2
12	226A (I3)–414R (C-term)	0.2	136T (I2)–379D (α4-β6)	91.5
13	229Q (I3)–406D (α5)	0.5	137S (I2)–379D (α4-β6)	94.4
14	229Q (I3)–410R (α5)	9.7	140K (I2)–376A (α4)	46.3
15	229Q (I3)–414R (C-term)	3.3	141Y (I2)–302W (α3)	1.3
16	237E (I3)–403D (α5)	65.6	141Y (I2)–379D (α4-β6)	86.9
17	263K (I3)–311S (α3-β5)	57.7	141Y (I2)–380G (α4-β6)	0.2
18	263K (I3)–312V (α3-β5)	0.2	141Y (I2)–382H (α4-β6)	90.9
19	263K (I3)–385Y (β6)	2.5	143S (I2)–383Y (α4-β6)	11.7
20	264F (I3)–385Y (β6)	95.4	145L (I2)–383Y (α4-β6)	93.8
21	267K (I3)–385Y (β6)	1.2	145L (I2)–414R (C-term)	0.2
22	267K (I3)–414R (C-term)	0.2	225E (I3)–308R (α3-β5)	86.3
23	267K (I3)–415Q (C-term)	0.1	226A (I3)–305R (α3)	94.9
24	270K (TMVI)–380G (α4-β6)	2.4	227K (I3)–305R (α3)	0.1
25	270K (TMVI)–381R (α4-β6)	0.1	229Q (I3)–303N (α3)	0.1
26	273K (TMVI)–379D (α4-β6)	24.6	229Q (I3)–305R (α3)	2.3
27	274T (TMVI)–417E (C-term)	0.1	229Q (I3)–308R (α3-β5)	27.6
28	328R (C-term)–381R (α4-β6)	0.1	263K (I3)–264N (α2-β4)	10.9
29	329S (C-term)–381R (α4-β6)	3.0	264F (I3)–305R (α3)	0.2
30	331D (C-term)–308R (α3-β5)	65.1	267K (I3)–264N (α2-β4)	9.7
31	331D (C-term)–309T (α3-β5)	99.7	268E (TMVI)–305R (α3)	67.2
32	331D (C-term)–310I (α3-β5)	60.6	332F (C-term)–416Y (C-term)	94.6
33	331D (C-term)–415Q (C-term)	98.8	333R (C-term)–417E (C-term)	96.0
34	333R (C-term)–417E (C-term)	5.3	333R (C-term)–419L (C-term)	0.1
35	335A (C-term)–308R (α3-β5)	0.1	336F (C-term)–416Y (C-term)	8.2
36	338E (C-term)–305R (α3)	67.0	338E (C-term)–56R (N-term)	0.2
37	338E (C-term)–308R (α3-β5)	18.5	346S (C-term)–53G (N-term)	6.0
38	346S (C-term)–304N (α3)	0.1	346S (C-term)–56R (N-term)	0.2

to a mean number of about three hydrogen bonds (Fig. 5a). In contrast, for the active $h\beta_2R$–$G\alpha_s$ complex, according to model I, during the 2.5 ns productive phase of the MD simulation a mean number of about 12 hydrogen bonds was detected (Fig. 5b). In general, these hydrogen bonds were established by 38 different amino acid interactions between the receptor and $G\alpha_s$ (Fig. 5c). Additionally, the frequency of hydrogen bond formation during the productive phase is given in Table 1. As indicated (Table 1, Fig. 5c), for model I, only about 11 distinct hydrogen bond interactions between the receptor and $G\alpha_s$ were observed during more than 50% of the simulation, and only about 6 during more than 80% of the simulation. For the active $h\beta_2R$–$G\alpha_s$ complex, according to model II, a mean number of about 15 hydrogen bonds was detected during the 2.5 ns productive phase of the simulation (Fig. 5d). These hydrogen bonds were established by 38 different amino acid interactions between the receptor and $G\alpha_s$ (Fig. 5e). However, only about 13 distinct hydrogen bond interactions between the receptor and $G\alpha_s$ were observed during more than 50% of the simulation, and about 11 during more than 80% of the simulation (Table 1, Fig. 5e). Figure 6 presents the hydrogen bond interactions between $h\beta_2R$ and $G\alpha_s$ with a frequency of >50% for models I and II.

In general, it should be taken into account that the productive phases of the MD simulations with 2.5 ns are too short to observe large conformational changes between the receptor and $G\alpha_s$. One reason for the short simulation time is the large size of the simulation box and computational capacity. On the other hand, large conformational changes between the receptor and G-protein may be expected for simulation times longer than 1,000 ns. Nowadays, such high cost simulations are almost unrealizable because of the long computation time. However, the MD simulations in this study were performed in order to gain information about the hydrogen bond network between the receptor and $G\alpha_s$, taking into account the natural surroundings, e.g., water and lipid bilayer, of the receptor–

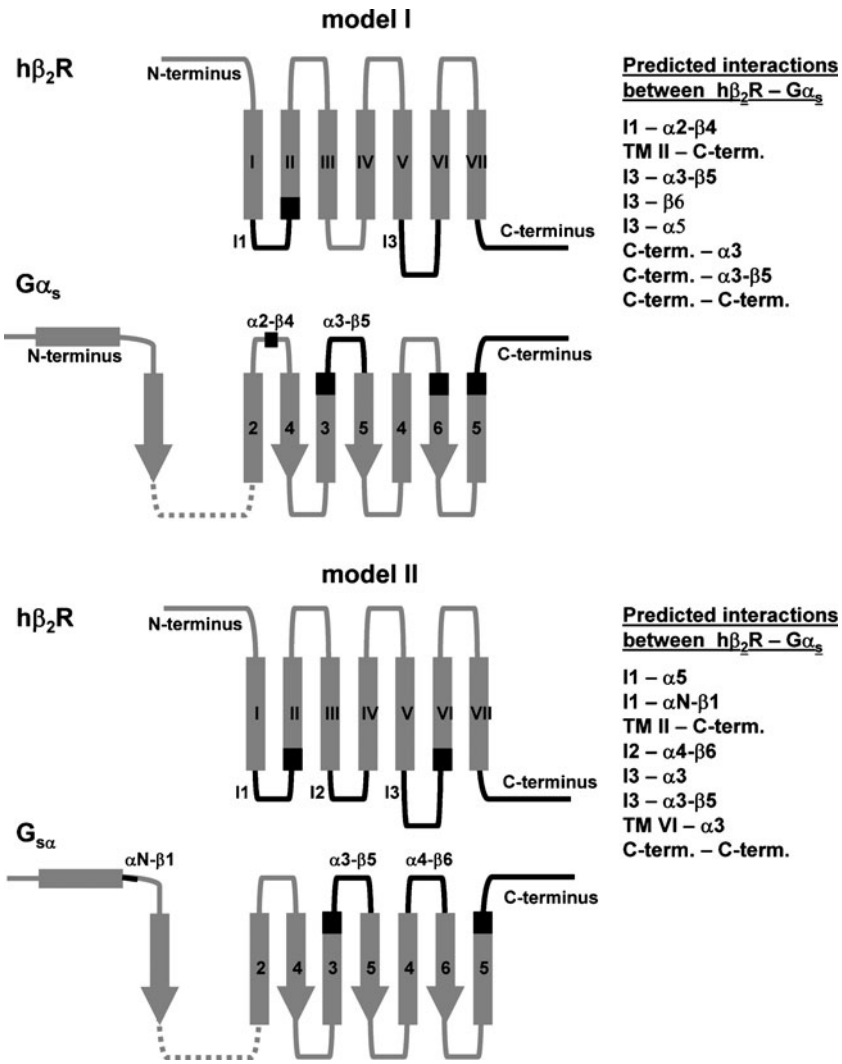

Fig. 6 Scheme for interactions between the receptor and Gα subunit according to models I and II. Predicted interactions between receptor and Gα subunit, based on the interactions detected for both energetically favored $h\beta_2R$–$G\alpha_s$ complexes, are indicated (only those with more than 50 % hydrogen bond interaction during the productive phase between at least two amino acids are included)

$G\alpha_s$ complex. The surroundings are necessary to avoid gas phase artifacts with regard to the hydrogen bond network in the receptor–$G\alpha_s$ complex. However, one should be aware that both interaction models are based primarily on gas phase scans of potential energy surface, and were refined by MD simulations including natural surroundings. On the other hand, it is important to gain more detailed insights into the interactions between GPCR and G-proteins on a molecular level. Thus, both models presented here may represent a good starting point for further studies.

Two models for receptor–G-protein interaction

The above calculations suggest that two different $h\beta_2R$–$G\alpha_s$ complexes are energetically favored (Fig. 4). In model I (Fig. 4), the N-terminus of $G\alpha_s$ is located below TM II of the receptor. Thus, the front of the $G\alpha_s$ subunit, interacting with $G\beta\gamma$, is located in the large space between TM VI and TM VII of the receptor. Therefore, it can be suggested that the long C-terminus of the receptor may be able to interact with the $G\beta\gamma$ subunit, subsequently leading to stabilization of the receptor–G-protein complex (Fig. 4). In contrast, in model II (Fig. 4), the N-terminus of $G\alpha_s$ is located between TM VI and TM VII of the receptor. Consequently, the front of the $G\alpha_s$ subunit, interacting with $G\beta\gamma$, is located below TM V and TM VI of the receptor. This suggests that the long I3 loop of the receptor can interact with the $G\beta\gamma$ subunit, again leading to stabilization of the receptor–G-protein complex (Fig. 4).

An additional analysis of the number of amino acids in the I3-loop or C-terminus of human aminergic GPCRs was performed (Fig. 7). This analysis revealed that the I3 loop of the $G\alpha_s$-coupling human aminergic GPCRs is significantly shorter than the C-terminus. In contrast, the I3 loop of the $G\alpha_i$-coupling human aminergic GPCRs is significantly longer than the C-terminus, whereas no significant difference in the length of I3 and the C-terminus was found for the $G\alpha_q$-coupling GPCRs. These data may indicate that the preferred orientation (model I or II, Fig. 4) between receptor and Gα-subunit is dependent on the length of the I3-loop or C-terminus. Furthermore, it may speculated that $G\alpha_s$ subunits interact with the receptor because of the longer C-terminus according to model I, whereas, according to model II, $G\alpha_i$ subunits couple to the corresponding receptor because of the longer I3-loop.

Comparison with experimental results

Several experimental and theoretical studies have analyzed the interactions between biogenic amine receptor and the Gα subunit. However, these have suggested only a few hints to distinct interactions between the receptor and $G\alpha_s$. Several experimental studies have suggested that the C-terminus [12, 17], α4–β6 loop [18–23], α3–β5 loop [24] and also the N-terminus [20, 25–28] of Gα subunits are relevant for the receptor–Gα interaction. Oldham and Hamm [29] point out that experimental results give information about a putative receptor–Gα binding surface. However, no single model can explain all the experimental results. Thus, one hypothesis is that these identified regions interact not simultaneously, but rather sequentially with the receptor [30]. Instead, based on our results, we present an alternative hypothesis, i.e., that there are two possible interaction models (model I and model II, Fig. 4), but which model is established is suggested to be dependent on the length of the I3-loop or C-terminus. It can be hypothesized that receptors with a long C-terminus interact with G-proteins according to model I (Fig. 4), and receptors with a long I3-loop follow model II (Fig. 4). It should be emphasized that this is only a hypothesis, since the conformation of long I3 loops or C-termini cannot be modeled due to the lack of an adequate crystal structure. However, the two-model hypothesis is based on geometrical considerations of the orientation of the receptor and Gα subunit with regard to each other. Further experimental and in silico studies should be performed to check this hypothesis. Additionally, it should be taken into account

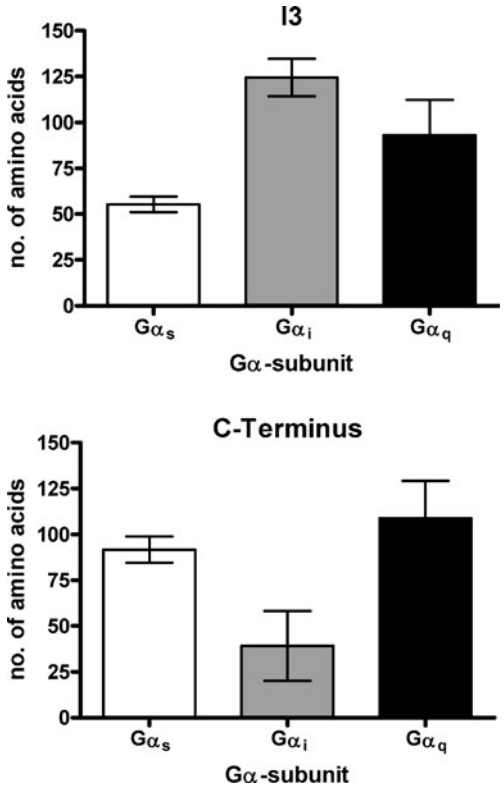

Fig. 7 Mean number of amino acids in the I3-loop or C-terminus of human aminergic G-protein-coupled receptors (GPCRs). The data are divided into receptors preferentially interacting with $G\alpha_s$, $G\alpha_i$ or $G\alpha_q$. The data shown are mean ± SEM

that knowledge of the receptor–G-protein interaction is based on a large number of different receptors, interacting with different Gα subunits. To verify our new, alternative hypothesis, extensive and systematic mutagenesis studies would have to be carried out with at least three receptor–G-protein systems, coupling to $G\alpha_i$, $G\alpha_q$ and $G\alpha_s$. The adrenergic receptors would be very suitable, since the α_1 adrenergic receptors interact with $G\alpha_q$, the α_2 adrenergic receptors with $G\alpha_i$ and the β adrenergic receptors with $G\alpha_s$. A comparison of our simulation results with experimental data shows in general good accordance. The alignment of the activated βh_2R in complex with the first 11 amino acids of $G\alpha_s$ with the corresponding crystal structure of opsin (3DQB.pdb) revealed an root mean square deviation of about 0.45 nm for the backbone atoms for model I and 1.01 nm for model II. Taking into account that our most favored structures are based on an energy-surface scan, the deviation for model I is rather small. In model II, the 11 amino acids of the C-terminus have a different orientation to the corresponding amino acids of 3DQB.pdb. Experimental studies have shown that the β_1-adrenergic receptor interacts preferentially with specific isoforms of the Gβ subunit [50]. Thus, both models, which suggest a distinct interaction between the C-terminus (model I, Fig. 4) of the I3-loop (model II, Fig. 4) of the receptor and the Gβ subunit, are in good agreement with these experimental results. Furthermore, experimental data suggest that even the I1-loop and C-terminus interact with G-proteins [51]. Both interaction models described here found an interaction between the I1-loop or C-terminus of the receptor with the G-protein. This in silico result is in good accordance with experimental results. Another experimental study showed that a peptide corresponding to the I3-loop of the α_2-adrenergic receptor can be crosslinked to the 60 C-terminal amino acids of the Gβ subunit [26, 52]. On the one hand, this experimental result accords well with model II (Fig. 4). On the other hand it agrees with our hypothesis that the orientation between receptor and G-protein is dependent on the length of the I3-loop or C-terminus. Based on the hypothesis introduced here, α_2-adrenergic receptors possessing a long I3-loop are suggested to interact with G-proteins according to model II (Fig. 4). Consequently, an interaction between the I3-loop and the Gβ subunit is expected. Summing up, it can be concluded that both receptor–G-protein interaction models presented here are in good accordance with experimental data. Although it has to be taken into account that both models are based on a gas phase scan of potential energy between the receptor and the Gα subunit, both final in silico models for the $h\beta_2R$–$G\alpha_s$ complexes, taking into account the lipid bilayer and solvent, may represent a good starting point for future theoretical and experimental studies.

Conclusions

Based on the crystal structure of activated opsin in complex with 11 amino acids of the G_t-C-terminus, two models of the active $h\beta_2R$ in complex with $G\alpha_s$ in the GTP-bound state were generated. The models, based on gas phase energy-surface scans, were refined by MD simulations including natural surroundings such as a POPC bilayer and water. In general, the two favored active $h\beta_2R$-$G\alpha_s$ models are in good accordance with several lines of experimental data described in the literature. Thus, both models may give detailed insight into the distinct interactions between $h\beta_2R$ and $G\alpha_s$. In addition, it may be hypothesized that two different interaction states between the receptor and G-protein exist depending on the length of the I3-loop or C-terminus. Furthermore, these models give very useful hints with regard to future mutagenesis studies for further experimental verification.

References

1. Wise A, Gearing K, Rees S (2002) Target validation of G-protein coupled receptors. Drug Discov Today 7:235–246
2. Kristiansen K (2004) Molecular mechanisms of ligand binding, signaling, and regulation within the superfamily of G-protein-coupled receptors: molecular modeling and mutagenesis approaches to receptor structure and function. Pharmacol Ther 103:21–80
3. Oldham WM, Hamm HE (2006) Structural basis of function in heterotrimeric G proteins. Q Rev Biophys 39:117–166
4. Pierce KL, Premont RT, Lefkowitz RJ (2002) Seven-transmembrane receptors. Nat Rev Mol Cell Biol 3:639–650
5. Gether U, Kobilka BK (1998) G Protein-coupled receptors. II. Mechanism of agonist activation. J Biol Chem 273:17979–17982
6. Palczewski K, Kumasaka T, Hori T, Behnke CA, Motoshima H, Fox BA, Le Trong I, Teller DC, Okado T, Stenkap RE, Yamamoto M, Miyano M (2000) Crystal structure of rhodopsin: a G protein-coupled receptor. Science 289:739–745
7. Cherezov V, Rosenbaum DM, Hanson MA, Rasmussen SGF, Thian FS, Kobilka TS, Choi HJ, Kuhn P, Weis WI, Kobilka BK, Stevens RC (2007) High-resolution crystal structure of an engineered human β_2-adrenergic G protein-coupled receptor. Science 318:1258–1265
8. Rasmussen SGF, Choi HJ, Rosenbaum DM, Kobilka TS, Thian FS, Edwards PC, Burghammer M, Ratnala VRP, Sanishvili R, Fischetti RF, Schertler GFX, Weis WI, Kobilka BK (2007) Crystal structure of the human β_2 adrenergic G-protein-coupled receptor. Nature 450:383–387
9. Rosenbaum DM, Cherezov V, Hanson MA, Rasmussen SGF, Thian FS, Kobilka TS, Choi HJ, Yao XJ, Weis WI, Stevens RC, Kobilka BK (2007) GPCR engineering yields high-resolution structural insights into β_2-adrenergic receptor function. Science 318:1266–1273
10. Warne T, Serrano-Vega MJ, Baker JG, Moukhametzianov R, Edwards PC, Henderson R, Leslie AG, Tate CG, Schertler GF (2008) Structure of a β_1-adrenergic G protein-coupled receptor. Nature 454:486–491
11. Jaakola VP, Griffith MT, Hanson MA, Cherezov V, Chien YET, Lane JR, Ijzerman AP, Stevens RC (2008) The 2.6 Å crystal

structure of a human A_{2A} adenosine receptor bound to an antagonist. Science 322:1211–1217
12. Scheerer P, Park JH, Hildebrand PW, Kim YJ, Krauß N, Choe HW, Hofmann KP, Ernst OP (2008) Crystal structure of opsin in its G-protein-interacting conformation. Nature 455:497–503
13. Tolkovsky AM, Levitzki A (1978) Mode of coupling between the β-adrenergic receptor and adenylate cyclase in turkey erythrocytes. Biochemistry 17:3795–3810
14. Gales C, van Durm JJJ, Schaak S, Pontier S, Percherancier Y, Audet M, Paris H, Bouvier M (2006) Probing the activation-promoted structural rearrangements in preassembled receptor-G-protein complexes. Nat Struct Mol Biol 13:778–786
15. Alves ID, Salamon Z, Varga E, Yamamura HI, Tollin G, Hruby VJ (2003) Direct observation of G-protein binding to the human δ-opioid receptor using plasmon-waveguide resonance spectroscopy. J Biol Chem 278:48890–48897
16. Alves ID, Salgado GFJ, Salamon Z, Brown MF, Tollin G, Hruby VJ (2005) Phosphatidylethanolamine enhances rhodopsin photoactivation and transducin binding in a solid supported lipid bilayer as determined using plasmon-waveguide resonance spectroscopy. Biophys J 88:198–210
17. Janz JM, Farrens DL (2004) Rhodopsin activation exposes a key hydrophobic binding site for the transducin a-subunit C terminus. J Biol Chem 279:29767–29773
18. Lichtarge O, Bourne HR, Cohen FE (1996) Evolutionarily conserved Gαβγ binding surfaces support a model of the G protein-receptor complex. Proc Natl Acad Sci USA 93:7507–7511
19. Mazzoni MR, Hamm HE (1996) Interaction of transducin with light-activated rhodopsin protects it from proteolytic digestion by trypsin. J Biol Chem 271:30034–30040
20. Onrust R, Herzmark P, Chi P, Garcia PD, Lichtarge O, Kingsley C, Bourne HR (1997) Receptor and βγ binding sites in the α subunit of the retinal G protein transducin. Science 275:381–384
21. Bae H, Anderson K, Flood LA, Skiba NP, Hamm HE, Graber SG (1997) Molecular determinants of selectivity in 5-hydroxytryptamine$_{1B}$ receptor-G protein interactions. J Biol Chem 272:32071–32077
22. Bae H, Cabrera-Vera TM, Depree KM, Graber SG, Hamm HE (1999) Two amino acids within the α4 helix of G_{i1}mediate coupling with 5-hydroxytryptamine$_{1B}$ receptors. J Biol Chem 274:14963–14971
23. Cai K, Itoh Y, Khorana HG (2001) Mapping of contact sites in complex formation between transducin and light-activated rhodopsin by covalent crosslinking: use of a photoactivatable reagent. Proc Natl Acad Sci USA 98:4877–4882
24. Grishina G, Bertlot CH (2000) A surface-exposed region of $G_s\alpha$ in which substitutions decrease receptor-mediated activation and increase receptor affinity. Mol Pharmacol 57:1081–1092
25. Hamm HE, Deretic D, Arendt A, Hargrave PA, Koenig B, Hofmann KP (1988) Site of G protein binding to rhodopsin mapped with synthetic peptides from the α subunit. Science 241:832–835
26. Taylor JM, Jacob-Mosier GG, Lawton RG, Remmers AE, Neubig RR (1994) Binding of an α_2 adrenergic receptor third intracellular loop peptide to Gβ and the amino terminus of Gα. J Biol Chem 269:27618–27624
27. Ho MK, Wong YH (2000) The amino terminus of $G\alpha_z$ is required for receptor recognition, whereas its α4/β6 loop is essential for inhibition of adenylyl cyclase. Mol Pharmacol 58:993–1000
28. Itoh Y, Cai K, Khorana HG (2001) Mapping of contact sites in complex formation between light-activated rhodopsin and transducin by covalent crosslinking: use of a chemically preactivated reagent. Proc Natl Acad Sci USA 98:4883–4887
29. Oldham WM, Hamm HE (2008) Heterotrimeric G protein activation by G-protein-coupled receptors. Nat Rev Mol Cell Biol 9:60–71
30. Herrmann R, Heck M, Henklein P, Henklein P, Kleuss C, Hofmann KP, Ernst OP (2004) Sequence of interactions in receptor-G protein coupling. J Biol Chem 279:24283–24290
31. Herrmann R, Heck M, Henklein P, Hofmann KP, Ernst OP (2006) Signal transfer from GPCRs to G proteins: role of the Gα N-terminal region in rhodopsin-transducin coupling. J Biol Chem 281:30234–30241
32. Fanelli F, Menziani C, Scheer A, Cotecchia S, de Benedetti PG (1999) Theoretical study of the electrostatically driven step of receptor-G protein recognition. Proteins 37:145–156
33. Fanelli F, Menziani C, Scheer A, Cotecchia S, de Benedetti PG (1999) Theoretical study on receptor-G protein recognition: New insights into the mechanism of the α_{1b}-adrenergic receptor activation. Int J Quant Chem 73:71–83
34. Greasley PJ, Fanelli F, Scheer A, Abuin L, Nenniger-Tosato M, de Benedetti PG, Cotecchia S (2001) Mutational and computational analysis of the α_{1B}-adrenergic receptor: involvement of basic and hydrophobic residues in receptor activation and G protein coupling. J Biol Chem 276:46485–46494
35. Oliveira L, Paiva PB, Paiva ACM, Vriend G (2003) Sequence analysis reveals how G protein-coupled receptors transduce the signal to the G protein. Proteins 52:553–560
36. Chou KC (2005) Coupling interaction between thromboxane A2 receptor and alpha-13 subunit of guanine nucleotide-binding protein. J Proteome Res 4:1681–1686
37. Raimondi F, Seeber M, de Benedetti PG, Fanelli F (2008) Mechanisms of the inter- and intramolecular communication in GPCRs and G proteins. J Am Chem Soc 130:4310–4325
38. Ballesteros JA, Shi L, Javitch JA JA (2001) Structural mimicry in G protein-coupled receptors: implications of the high-resolution structure of rhodopsin for structure-function analysis of rhodopsin-like receptors. Mol Pharmacol 60:1–19
39. Wall MA, Coleman DE, Lee E, Iniguez-Lluhi JA, Posner BA, Gilman AG, Sprang SR (1995) The structure of the G protein heterotrimer $G\alpha_{i1}\beta_1\gamma_2$. Cell 83:1047–1058
40. Sunahara RK, Tesmer JJ, Gilman AG, Sprang SR (1997) Crystal structure of the adenylyl cyclase activator Gsα. Science 278:1943–1947
41. Wall MA, Coleman DE, Lee E, Iniguez-Lluhi JA, Posner BA, Gilman AG, Sprang SR (1995) The structure of the G protein heterotrimer Gi alpha beta 1 gamma 2. Cell 83:1047–1058
42. Van der Spoel D, Lindahl E, Hess B, Groenhof G, Mark AE, Berendsen HJC (2005) GROMACS: fast, flexible, and free. J Comput Chem 26:1701–1718
43. Oostenbrink C, Villa A, Mark AE, van Gunsteren WF (2004) A biomolecular force field based on the free enthalpy of hydration and solvation: the GROMOS force-field parameter sets 53A5 and 53A6. J Comput Chem 25:1656–1676
44. Berendsen HJC, Postma JPM, van Gunsteren WF, Hermans J (1981) In: Pullmann BE (ed) Intermolecular forces. Dordrecht, Reidel, p 331
45. Essman U, Perera L, Berkowitz ML, Darden T, Lee H, Pedersen LG (1995) A smooth particle mesh Ewald method. J Chem Phys 103:8577–8593
46. Berendsen HJC, Postma JPM, van Gunsteren WF, DiNola A, Haak JR (1984) Molecular dynamics with coupling to an external bath. J Chem Phys 81:3684–3690
47. Nose S (1984) A molecular-dynamics method for simulations in the canonical ensemble. Mol Phys 52:255–278
48. Hoover WG (1985) Canonical dynamics—equilibrium phase-space distributions. Phys Rev A 31:1695–1697

49. Parrinello M, Rahman A (1981) Polymorphic transitions in single crystals—a new molecular-dynamics method. J Appl Phys 52: 7182–7190
50. McIntire WE, MacCleery G, Garrison JC (2001) The G protein β subunit is a determinant in the coupling of G_s to the β_1-adrenergic and A_{2a} adenosine receptors. J Biol Chem 276: 15801–15809
51. Wess J (1997) G-protein-coupled receptors: molecular mechanisms involved in receptor activation and selectivity of G-protein recognition. FASEB J 11:346–354
52. Taylor JM, Jacob-Mosier GG, Lawton RG, van Dort M, Neubig RR (1996) Receptor and membrane interaction sites on Gβ. A receptor-derived peptide binds to the carboxyl terminus. J Biol Chem 271:3336–3339